Voxel Cores: Efficient, robust, and provably good approximation of 3D medial axes

YAJIE YAN, Washington University in St. Louis, USA
DAVID LETSCHER, St. Louis University, USA
TAO JU, Washington University in St. Louis, USA

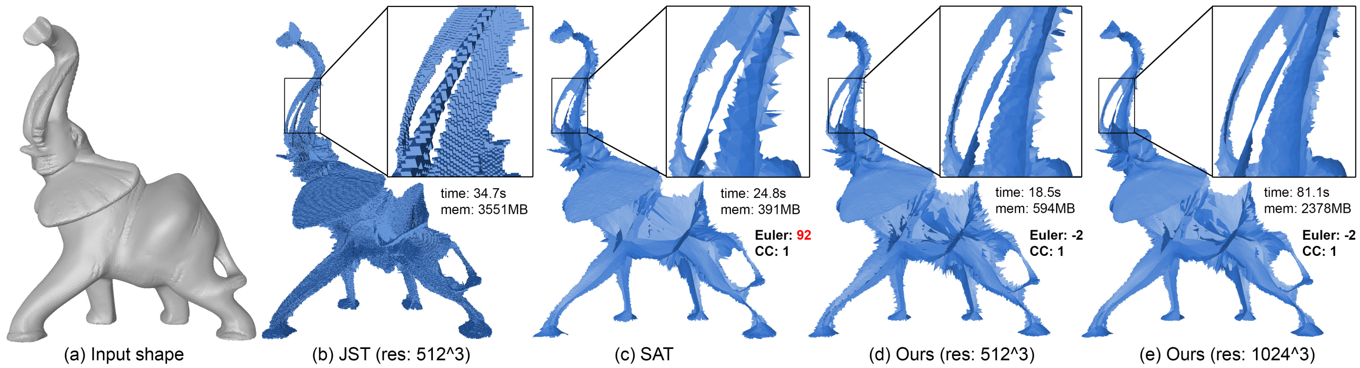

Fig. 1. Approximations of medial axis of the Elephant (a) using the voxel-based method of [Jalba et al. 2016] (noted as JST) (b), the sampling-based method of [Amenta and Kolluri 2001] (as implemented in SAT [Miklos et al. 2010]) (c), and our method at two different voxelization resolutions (d,e). Topological numbers including the Euler characteristic ("Euler") and number of connected components ("CC") are noted for methods other than JST. Our method requires significantly less resources than JST, which is unable to handle resolutions higher than 512^3 for this input, and produces visually comparable results to SAT but without its topological errors (as evident in the incorrect Euler characteristic).

We present a novel algorithm for computing the medial axes of 3D shapes. We make the observation that the medial axis of a voxel shape can be simply yet faithfully approximated by the interior Voronoi diagram of the boundary vertices, which we call the *voxel core*. We further show that voxel cores can approximate the medial axes of any smooth shape with homotopy equivalence and geometric convergence. These insights motivate an algorithm that is simple, efficient, numerically stable, and equipped with theoretical guarantees. Compared with existing voxel-based methods, our method inherits their simplicity but is more scalable and can process significantly larger inputs. Compared with sampling-based methods that offer similar theoretical guarantees, our method produces visually comparable results but more robustly captures the topology of the input shape.

CCS Concepts: • **Computing methodologies → Shape analysis**;

Additional Key Words and Phrases: medial axis, shape analysis, voxelization, Voronoi diagrams

Authors' addresses: Yajie Yan, Washington University in St. Louis, 1 Brookings Dr. St. Louis, MO, 63130, USA; David Letscher, St. Louis University, 1 N. Grand Blvd. St. Louis, MO, 63130, USA; Tao Ju, Washington University in St. Louis, 1 Brookings Dr. St. Louis, MO, 63130, USA.

0730-0301/2018/8-ART44 $15.00
https://doi.org/10.1145/3197517.3201396

ACM Reference Format:
Yajie Yan, David Letscher, and Tao Ju. 2018. Voxel Cores: Efficient, robust, and provably good approximation of 3D medial axes. *ACM Trans. Graph.* 37, 4, Article 44 (August 2018), 13 pages. https://doi.org/10.1145/3197517.3201396

1 INTRODUCTION

The medial axis [Blum 1967] is a fundamental geometric structure in computer graphics and computer vision. The medial axis $\mathcal{M}$ of a shape O is simply defined as the set of points in O with two or more nearest neighbors on the boundary of O (see a more formal definition in Section 3.1). The usefulness of the medial axis arises from its many topological and geometric properties. Topologically, $\mathcal{M}$ is thin (i.e., at least one dimension thinner than O) and homotopy equivalent to O. Geometrically, $\mathcal{M}$ is centered in O and captures the protrusions and components of O. As a result, medial axes have been used in approximating, simplifying, and analyzing shapes. They have also become the foundation for other skeletal shape descriptors [Tagliasacchi et al. 2016].

While simply defined, the medial axis is notoriously difficult to compute. In 3D, the medial axes of most common shapes are complex networks of curved sheets. While methods that compute such networks precisely exist [Culver et al. 2004], they are limited to rather simple shapes due to the high computational cost. To be able to handle complex, real-world data, most existing methods resort to approximations. The goal of approximation is therefore to retain as many properties (both topologically and geometrically) of the medial axis as possible while being able to scale to large inputs.

Existing approximation methods of 3D medial axes mostly fall into two categories, each hitting a different balance among scalability, robustness, and theoretical soundness (see Section 2 for a detailed review):

- *Voxel-based* methods operate on a shape represented by a union of voxels. Such shapes may directly come from the input (e.g., segmented MRI or CT scans) or can be converted from a boundary representation (e.g., by voxelization). Voxel-based methods are generally easy to implement and numerically robust. However, they need to store and process a large number of voxels interior to the shape, which is expensive in both time and memory (Figure 1 (b)). Furthermore, there is no theoretical guarantee when it comes to approximating the medial axis of non-voxel (e.g., smooth) shapes.
- *Sampling-based* methods consider point samples on the shape boundary and are often based on the Voronoi diagram of these samples. As the samples are taken on the boundary (as opposed to interior voxels), these methods are more scalable than voxel-based methods. While these methods can be equipped with strong theoretical guarantees when the shape boundary is smooth (e.g., C^2), they often involve highly non-trivial geometric computations (e.g., multiple passes of Voronoi computations and geometric intersections) that are numerically sensitive, which can lead to numerous topological errors on the resulting approximations (Figure 1 (c)).

In this work, we present a new method for approximating the medial axes of 3D shapes that is simple, efficient, numerically robust, and equipped with theoretical guarantees for both voxel and smooth shapes. Our method rests on two novel insights on voxel shapes. First, we show that the medial axis of a voxel shape can be well approximated, both topologically and geometrically, by the interior Voronoi diagram of boundary vertices. We call this approximation the *voxel core*. Second, we show that the voxel core can provide a topologically correct and geometrically convergent approximation of the medial axis of any smooth (C^2) shape given a voxelization of the shape at sufficiently high resolutions.

These observations lead to a simple approximation method that can be applied to both voxel shapes (natively) and boundary representations (via voxelization). Compared with current voxel-based methods, our method is more scalable, because its complexity scales with only the number of boundary voxels, and is additionally equipped with convergence guarantees for smooth shapes. Compared with existing sampling-based methods that share similar theoretical warranties, our method is not only simpler to implement but is also numerically robust, since the only non-trivial computation is computing the Voronoi diagram of points with integer coordinates.

1.1 Contributions

We make several theoretical and practical contributions in this work.

First, we show that the interior Voronoi diagram of voxel shapes (the *voxel core*) keeps all essential properties of the medial axis: it is thin (at most two-dimensional), enclosed in and homotopy equivalent to the voxel shape, and less than one voxel away from the medial axis of the voxel shape. This result contrasts the well-known fact that the Voronoi diagram of points samples of a smooth 3D shape is not a converging approximation of the shape's medial axis [Amenta et al. 2001].

Second, we show that the voxel core is a theoretically sound approximation of medial axes of smooth (C^2) shapes when used in conjunction with voxelization. Our work draws upon results from two bodies of literature, one on the geometric and topological properties of digitizations [Lachaud and Thibert 2016; Stelldinger et al. 2007] and one on medial axis approximation with noisy point samples [Chazal and Lieutier 2005, 2008]. Specifically, we give conditions on voxel sizes under which the voxel core preserves the homotopy of the smooth shape, and we show that an arbitrarily large subset of the voxel core converges onto the medial axis of the smooth shape as the voxel size tends to zero.

Third, and practically, we present an efficient and robust algorithm for computing 3D medial axes. The scalability of the algorithm allows it to handle much larger voxel shapes (e.g., 1024^3 and above) than existing voxel-based methods, making it suitable for processing high-resolution biomedical imaging data. When given other boundary representations (e.g., meshes), the results of our method are visually comparable to existing sampling-based methods but free of topologically errors caused by numerical sensitivity. Furthermore, even though our method considers a "noisy" sampling of the smooth shape, we observe that it requires fewer samples, and hence is more efficient, than existing sampling-based methods for capturing fine topological details (e.g., a narrow connection). The algorithm is also simple to implement; most of the computations are done using existing packages (e.g., for voxelization and Voronoi diagram computation).

2 RELATED WORKS

We review representative works on approximating the medial axis. As medial axes are sensitive to boundary perturbations, a closely related problem is identifying stable and significant parts of the medial axis (known as regularization), and we refer readers to recent works [Li et al. 2015; Miklos et al. 2010; Yan et al. 2016] for reviews. Note that many regularization methods work by pruning noisy branches of the medial axis [Li et al. 2015; Yan et al. 2016], which requires an initial approximation of the medial axis. We refer readers to excellent survey materials [Siddiqi and Pizer 2008; Tagliasacchi et al. 2016] for more extensive discussions on medial axes, skeletal shape descriptors and other medial representations.

2.1 Algebraic methods

These methods attempt to create an accurate, analytic representation of the medial axis from a given boundary representation, such as polyhedra [Culver et al. 2004; Milenkovic 1993; Sherbrooke et al. 1996], CSG [Hoffmann 1990], and free-form surfaces [Musuvathy et al. 2011; Ramanathan and Gurumoorthy 2010]. They usually work by tracing the features of the medial axes (e.g., seams and junctions) from the shape boundary inward. Due to the need to solve (often degenerate) systems of non-linear functions, implementing these methods in a numerically robust way is both algorithmically challenging and computationally expensive, which limits the application of these methods to small inputs (e.g., meshes with hundreds of polygons).

2.2 Voxel-based methods

These methods take a voxel shape and identify a subset of the voxels that share similar properties as the medial axis, such as being thin, centered, and preserving both the shape's topology and shape components [Saha et al. 2016; Sobiecki et al. 2014]. The restriction to a finite set of voxels lends simplicity and robustness to these methods. In particular, preserving the topology can be easily achieved by a thinning process that strips away layers of voxels while keeping those voxels that are critical for retaining topology [Bertrand and Malandain 1994; Saha and Chaudhuri 1994].

Many voxel-based methods are guided by a non-Euclidean distance metric that can be locally evaluated, such as Manhattan distance [Palágyi and Kuba 1999; Tsao and Fu 1981], chamfer distance [Pudney 1998], and <3,4,5> distance [Arcelli et al. 2011]. While efficient to evaluate, these metrics are dependent on the orientation of the voxel grid, making the results sensitive to affine transformations of the shape. More accurate and transformation-invariant results can be obtained by computing the Euclidean distance field [Arcelli and di Baja 1993; Ge and Fitzpatrick 1996; Hesselink and Roerdink 2008; Rumpf and Telea 2002], the derived gradient field [Siddiqi et al. 2002], or more global shape information [Jalba et al. 2016; Reniers et al. 2008]. However, computing these metrics increases both the running time and memory storage per voxel. In general, the complexity of any voxel-based method is linear to the total number of voxels, which is cubic to the resolution of the voxel grid. In practice, we have noticed that such complexity makes current methods infeasible for processing volumes with resolutions of 1024^3 or above, which are not uncommon in practice (e.g., voxelization of highly complex models with fine geometric features, or high-resolution biomedical data).

Voxels can also serve as a spatial partitioning structure to accelerate algebraic methods. Such methods search for features of the medial axis within each voxel [Foskey et al. 2003; Lee and Lee 1997], subdividing when necessary [Etzion and Rappoport 2002; Stolpner and Siddiqi 2006; Sud et al. 2006]. While these methods are more efficient than the algebraic methods mentioned above, their computational cost remains high since it scales with the product of the number of boundary elements and the number of voxels.

Voxel-based methods are often used to approximate the medial axis of non-voxel shapes (e.g., meshes) via voxelization. However, a theoretical understanding of the quality of such approximation is still missing. In particular, it is not clear what voxel resolution is required (or whether such resolution exists) so that the voxel-based medial axis preserves the topology of the shape, or how close the voxel-based approximation is to the true medial axis of the shape as a function of the voxel resolution.

2.3 Sampling-based methods

These methods place point samples on or around the shape's boundary and consider either a subset of the Voronoi diagram of these samples or some derivative structures. The use of boundary samples, as opposed to interior voxels, make these methods more efficient and scalable than voxel-based methods. The main challenge is offering assurance of the quality of the resulting approximation, particularly its proximity to the medial axis and topology. Note that, for 2D smooth shapes, the subset of Voronoi diagram of boundary samples interior to the shape already provides topological and geometrically converging approximation to the medial axis [Brandt and Algazi 1992]. However, this simple approximation does not work for smooth 3D shapes, due to existence of "sliver" tetrahedra in Delaunay triangulation of boundary samples, which lead to Voronoi vertices close to the boundary but far away from the medial axis [Amenta et al. 2001].

Existing 3D sampling-based methods offer different levels of guarantees on their approximations, and stronger guarantees generally imply more complex and numerically fragile implementations. Ma et al. [2012] and Jalba et al. [2013] locate points of maximal balls given normals at the sample points. However, they do not provide any error analysis of their approximation nor any guarantees on topology.

Attali and Montanvert [1996] and Dey and Zhao [Dey and Zhao 2003] consider a subset of the Voronoi diagram of the samples that satisfy an angle criteria. The subset is shown to converge geometrically to the medial axis of a smooth shape as the sampling density increases [Dey and Zhao 2003], but no assurance is provided on whether the subset preserves the topology of the medial axis (our experiments found that this subset tends to have many holes and isolated components).

Giesen et al. [Giesen et al. 2006] show that the unstable manifold of the Voronoi diagram has the same topology as the smooth shape at sufficiently high sampling density, and this manifold can be extended to include the angle-filtered subset in [Dey and Zhao 2003] to achieve bounded approximation of the medial axis. However, computing the unstable manifold is a numerically challenging task, and existing implementations [Cazals et al. 2008] are extremely time consuming (taking hours for over $50k$ points).

Amenta et al. [Amenta et al. 2001] considers "poles" of Voronoi diagram and show that the power shape of these poles converge both geometrically and topologically to the medial axis of a smooth shape as the sampling density increases. However, the power shape is not always thin, and in practice it contains a large number of rather flat tetrahedra. A thin and topology-preserving approximation can be obtained by replacing the power shape with the medial axis of the union of the polar balls [Amenta and Kolluri 2001; Tam and Heidrich 2003]. While theoretically sound, such approximation requires multiple passes of Voronoi computations as well as geometric intersections, which are difficult to implement in a numerically robust manner. We know of only one implementation [Miklos et al. 2010], which we found to routinely produce topological errors (e.g., duplicate elements and closed "pockets"; see Figure 1).

Comparing with these methods, our method for approximating the medial axis of smooth shapes is equipped with equally strong theoretical guarantees (in both topology and proximity) but is simpler to implement and numerically robust. Our theoretical analysis builds on the results of Chazal and Lieutier [2005; 2008], who showed that a subset of the Voronoi diagram of a sufficiently close and dense noisy sampling retains the topology of the shape and converges to the medial axis geometrically (see more detailed discussion in Section 3.1). In the context of their work, our contribution is presenting sampling conditions in terms of the voxel size that are necessary for our particular approximation (voxel core) to achieve homotopy equivalence and geometric convergence.

3 THEORY

In this section, we present our theoretical results on approximating the medial axes of voxel shapes and smooth shapes. These results motivate and guide our algorithm design in the next section. After reviewing a few key concepts (Section 3.1), we will introduce voxel cores and show that they are excellent surrogates of the medial axes of voxel shapes (Section 3.2). We next show that the voxel cores are also good approximations of the medial axes of smooth shapes via voxelization (Section 3.3).

While the results are presented for voxel shapes in 3D, we have verified that similar results hold for “pixel shapes” in 2D as well. We do not present the 2D results here, but will use 2D examples for illustrating the concepts. Due to space limit, we only present here selected proofs; the remaining proofs and supporting lemmas are included in the Supplementary Materials.

3.1 Preliminaries

Medial axis: Consider a bounded open set O of $\mathbb{R}^n$. The *medial axis* $\mathcal{M}$ is the set of points of O that are closest to two or more points on the boundary of O, or ∂O (see insert for an illustration). More precisely, for any $x \in O$, let $\Gamma(x)$ be the set of its closest points on the boundary,

$$\Gamma(x) = \{y \in \partial O \mid d(x, y) = d(x, \partial O)\}$$

where d is the Euclidean distance. The medial axis is defined as

$$\mathcal{M} = \{x \in O \mid |\Gamma(x)| \geq 2\}$$

The medial axis of an n-dimensional set is generally a $(n-1)$-dimensional structure. For $n = 3$, $\mathcal{M}$ is made up of 2-dimensional manifolds glued at non-manifold curves (called seams) and points (called junctions). Since each point of $\mathcal{M}$ is equidistant to at least two locations on the boundary, $\mathcal{M}$ is centered within the shape and captures local symmetries. The medial axis has also been shown to be *homotopy equivalent* to the open set O [Lieutier 2003], which means that the two structures have the same set of topological features, such as holes, tunnels, and connected components.

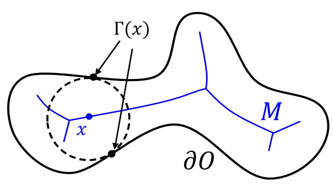

Hausdorff distance and λ-medial axis: To measure the distance between two compact sets A, B, we use the symmetric Hausdorff distance d_H defined as

$$d_H(A, B) = \max(\sup_{x \in A} d(x, B), \sup_{x \in B} d(x, A))$$

Chazal and Lieutier [2005] show that, even though the medial axis is highly sensitive to boundary perturbations, a subset of the medial axis enjoys certain stability properties when the perturbation is bounded by the Hausdorff distance. In particular, they define the *λ-medial axis*, $\mathcal{M}_\lambda$, as consisting of points $x \in \mathcal{M}$ such that the smallest enclosing ball of the nearest boundary point set $\Gamma(x)$ has a radius of λ or greater. They showed that, for two open sets O, O' whose Hausdorff distance is ϵ, the λ-medial axis of one set is within a bounded distance from the medial axis of the other set, for sufficiently large values of λ. We will build on their results to show the geometric convergence of our approximation for medial axes of smooth shapes.

Voronoi diagram and Delaunay triangulation: Our method is based on these two classical geometric structures. We briefly review their definition and key properties, and refer to standard textbooks in computational geometry for thorough discussions. Given a finite set of points P in $\mathbb{R}^n$, the *Voronoi cell* of a point $p \in P$ consists of all points in $\mathbb{R}^n$ whose distance to p is no greater than to any other point of P. The *Voronoi diagram* of P, $VD(P)$, consists of points in $\mathbb{R}^n$ that are closest to two or more points of P. Points in $VD(P)$ form (closed) elements at different dimensions $d = 0, \ldots, n$, which we call Voronoi vertices, edges and faces for $d = 0, 1, 2$.

The *Delaunay triangulation*, denoted by $DT(P)$, is another complex with a dual structure to the Voronoi diagram. Each d-dimensional Voronoi element e is dual to a $(n-d)$-dimensional Delaunay element $\widetilde{e}$, defined as the convex hull of points in P whose Voronoi cell have e on its boundary. The vertices of $\widetilde{e}$ lie on an n-dimensional *empty ball* that is centered on the Voronoi element e and does not contain any other point of P in its interior. When all points P are in general position (i.e., no 4 co-circular points, or 5 co-spherical points, etc.), the Delaunay triangulation is a simplicial complex. That is, each d-dimensional Delaunay element is the convex hull of exactly $(d+1)$ points. However, when P assume integer coordinates (e.g., voxel vertices), their positions are longer general, and $DT(P)$ may consist of non-simplicial elements such as 2-dimensional polygons and 3-dimensional polyhedra.

3.2 The voxel core

We consider the tiling of $\mathbb{R}^3$ by cubes of equal sizes, each called a *voxel*. The boundary elements of a voxel are called the voxel vertices, edges and faces. A *voxel shape* is the interior of the union of a finite set of voxels. By this definition, a voxel shape is an *open set* that does not include the vertices, edges, or faces on the boundary of the union. Note that the voxel shape may have a different topology from the union of voxels. In the 2D example of Figure 2 (a), the union of the voxels encloses a cavity that is disconnected from the outside, but such cavity does not exist in the voxel shape. As we shall see, considering the open set as the voxel shape is critical for establishing the topological equivalence with our medial axis approximation. Note that a voxel shape is consistent with 6-connectivity in digital topology [Klette and Rosenfeld 2004].

3.2.1 Definition. To motivate our definition of the voxel core, we start with the following key observation of a voxel shape. Given a voxel shape O, we denote by B the set of vertices, edges, and faces on the boundary ∂O, and by P the vertices in B.

Theorem 3.1. *The boundary set B is a subset of the elements in the Delaunay triangulation $DT(P)$.*

Proof. It suffices to show that each boundary element $e \in B$ has an empty ball. We only need to consider the case where e is an edge or face as we are in $\mathbb{R}^3$. In either case, we construct the ball

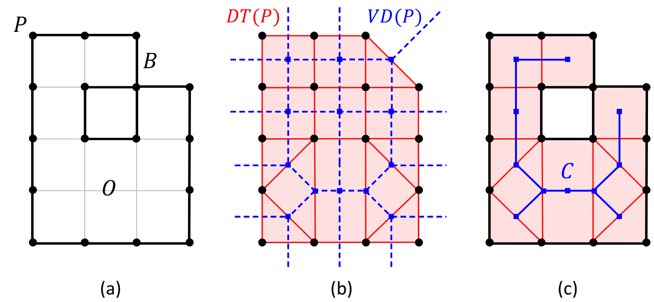

Fig. 2. Illustration of voxel core in 2D. (a) A voxel shape O with boundary set B (thick outline) and boundary vertices P (dots). (b) The Delaunay triangulation $DT(P)$ (red edges and pink cells) and Voronoi diagram $VD(P)$ (blue). (c) Subset of $DT(P)$ intersecting O and their dual Voronoi elements, which make up the voxel core C (blue).

as the smallest circumscribing sphere of e, which is centered at the midpoint of the edge or the centroid of the face. The ball is empty because 1) all vertices of e are on the ball, and 2) no other vertices in P are closer to the ball center than the vertices of e (see Lemma 1.1 in Supplementary Materials).[1] □

Note that his property does not hold if B is a general 3D polyhedron: not every edge and face of a polyhedron is contained in the Delaunay triangulation of the polyhedron's vertices. In the simple 2D example in Figure 2 (a,b), one observes that the boundary set B (thick outline in (a)) is contained in $DT(P)$ (red and pink in (b)).

As a result of Theorem 3.1, the boundary set B partitions the remainder of the Delaunay triangulation into two subsets, one subset making up the closure of O and the other subset making up the complement of O. The voxel core is defined by the dual Voronoi elements of the first subset (Figure 2 (c)):

Definition 3.2. The ***voxel core***, C, of a voxel shape O with boundary vertices P is the subset of the Voronoi elements whose dual Delaunay elements in $DT(P)$ have non-empty intersections with O.

3.2.2 *Properties.*

While simply defined, the voxel core C inherits several key properties of the medial axis $\mathcal{M}$ of the voxel shape O: it is thin (i.e., void of 3-dimensional cells), homotopy equivalent to O (i.e., sharing the same set of holes, tunnels, and components), and completely enclosed within O. In addition, C is less than a voxel away from $\mathcal{M}$. These properties are detailed next.

Thinness: The thinness of the voxel core is a direct consequence of its duality with Delaunay triangulation. Note that all vertices of $DT(P)$ lie on the boundary ∂O. Since C is dual to elements of $DT(P)$ that intersect O, no element of C is dual to a 0-dimensional vertex. As a result,

Theorem 3.3. *C has no 3-dimensional cells.*

The voxel core is usually a 2-dimensional complex, but it may also contain edges that are not shared by any faces (e.g., when O is

[1] We have in fact shown that B is a subset of the *Gabriel graph* of P, which is in turn a subset of $DT(P)$.

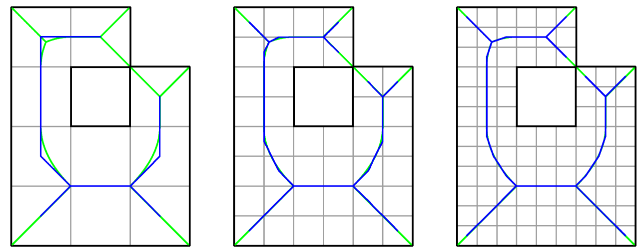

Fig. 3. Voxel core in 2D (blue) after increasing levels of voxel subdivision. Observe that it converges to the medial axis (green) of the voxel shape.

a one-voxel thick tube) or even isolated vertices (e.g., when O is a single voxel).

Homotopy equivalence: The duality also allows us to relate the topology of the voxel core with that of the voxel shape:

Theorem 3.4. *C is homotopy equivalent to O.*

The proof, given in the Supplementary Materials, is based on the *nerve theorem* [Björner et al. 1985], which establishes the topological equivalence between a cell complex and its dual. Note that the voxel core preserves the topology of the open set but not its closure (the union of voxels). Back to the example of Figure 2, the voxel core C (blue line in (c)) is a simply connected graph, whereas the union of voxels forms a loop that disconnects the complement into two components.

Proximity: We show that the voxel core C is close to the medial axis $\mathcal{M}$ by bounding the Hausdorff distance between the two sets. Let h be the length of a voxel edge (which we will refer to as the voxel size). We can show that:

Theorem 3.5. *$d_H(C, \mathcal{M}) \leq \frac{\sqrt{3}}{2}h$. More specifically,*

(1) *For any $x \in C$, $d(x, \mathcal{M}) \leq \frac{1}{4}h$.*
(2) *For any $x \in \mathcal{M}$, $d(x, C) \leq \frac{\sqrt{3}}{2}h$.*

The proof is given in the Supplementary Materials. The proof proceeds by moving a point from C (resp. $\mathcal{M}$) in a well-chosen direction so that it can not travel for more than a certain distance before hitting $\mathcal{M}$ (resp. C).

The distance bound leads to a simple method, by voxel subdivision, for computing a converging approximation to the medial axis of a voxel shape. Consider a new voxel shape O' created by subdividing each voxel in O into $k \times k \times k$ voxels of size h/k. Since O' covers the same open set as O, the two voxel shapes share the same medial axis $\mathcal{M}$. On the other hand, the Hausdorff distance between the voxel core C' of O' and $\mathcal{M}$ is reduced to $(\sqrt{3}/2k)h$. Figures 3,4 demonstrate the effect of voxel subdivision on the voxel core in 2D and 3D.

Enclosure: Finally, we show that the voxel core, just like the medial axis, lies completely inside the shape. As we shall see, this property also leads to an simple way to check if a Voronoi element is in the voxel core (which we call the *in-core* check).

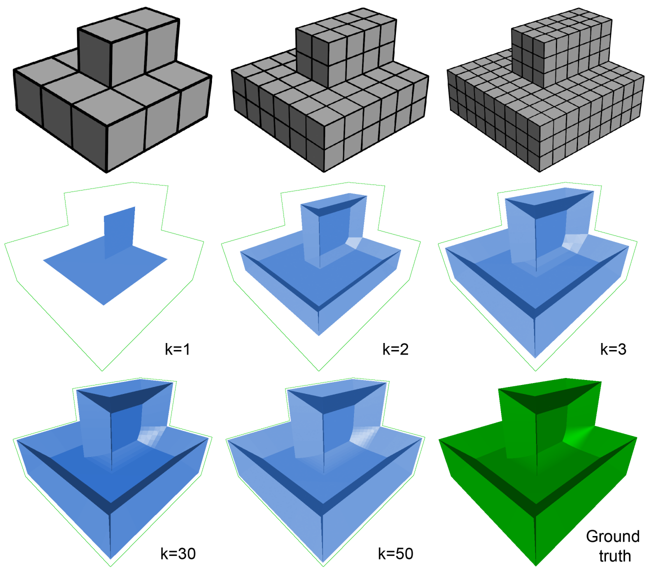

Fig. 4. Voxel core (middle and bottom rows) of a 3D voxel shape after increasing levels of voxel subdivision (showing only first two levels in top row). Observe that it converges to the medial axis (green) of the voxel shape.

We first make another observation of the boundary set B. In particular, the Voronoi elements dual to B, denoted by $\widetilde{B}$, are the *only* Voronoi elements that intersect the boundary B:

Lemma 3.6. *An element $e \in VD(P)$ has a non-empty intersection with B if and only if $e \in \widetilde{B}$.*

Proof. We first show sufficiency. Consider an element $e \in \widetilde{B}$, and let $\widetilde{e}$ be its dual Delaunay element (note that $\widetilde{e} \in B$). If $\widetilde{e}$ is a vertex, it is contained in e. If $\widetilde{e}$ is an edge, the argument in the proof of Theorem 3.1 shows that the midpoint of $\widetilde{e}$ is the center of an empty ball for $\widetilde{e}$, and hence the midpoint lies on e. Similarly, if $\widetilde{e}$ is a face, its centroid lies on e. In each case, e has a non-empty intersection with B. To show necessity, consider an element $e \in VD(P)$ that intersects B at point x. Let f be the lowest-dimension element of B that contains x. The vertices in P closest to x must be vertices of f (see Lemma 1.1 in Supplementary Materials). Hence e is dual to either f or a boundary element of f. Since f and all of its boundary elements are in the boundary set B, we have $e \in \widetilde{B}$. □

This observation allows us to prove the enclosure property:

Theorem 3.7. *$C \subset O$.*

Proof. By Theorem 3.4, each connected component of O is captured by a connected component of C. Since C and $\widetilde{B}$ have no elements in common, by Lemma 3.6, C does not intersect B. Hence, for a component of O, say O_1, its corresponding component of C, say C_1, either lies completely inside O_1 or has no intersection with O_1. To prove the theorem, it suffices to show that some element of C_1 lies in O_1. Consider a face f on the boundary of O_1. f bounds two Delaunay cells, one of which is in O_1, which we denote by t. The dual Voronoi edge of f, $\widetilde{f}$, has two vertices, one of which is due to t, or $\widetilde{t}$. Since t is inside O_1, $\widetilde{t}$ is in C_1. On the other hand, by Lemma 3.6 and the argument therein, the Voronoi edge $\widetilde{f}$ intersects f but no other faces on the boundary of O_1. Hence $\widetilde{t}$ lies inside O_1, and so is the entirety of C_1. □

By the argument in the proof of Theorem 3.7, the dual Voronoi element of a face in B is an edge with precisely one vertex in O. Since every element in $\widetilde{B}$ contains some Voronoi edge, it follows that all elements of $\widetilde{B}$ are "mixed", meaning they have vertices both inside and outside O. As the vertex core C is disjoint from $\widetilde{B}$ and lies inside O, we conclude that C is precisely the subset of $VD(P)$ whose vertices lie completely inside O. This conclusion leads to a simple way to perform the in-core check: *a Voronoi element of $VD(P)$ is in the voxel core C if and only if its vertices lie in the voxel shape O.*

Combining the statement above and Theorem 3.7 (and the argument in the proof), we conclude our discussion of the voxel core by showing three equivalent definitions of the voxel core:

Corollary 3.8. *The following three sets are identical to the voxel core C:*

(1) *Elements of $VD(P)$ that are dual to elements of $DT(P)$ that intersect O.*
(2) *Elements of $VD(P)$ that lie completely in O.*
(3) *Elements of $VD(P)$ whose vertices lie in O.*

3.3 Approximating medial axes of smooth shapes

We next consider approximating the medial axis of a smooth shape by the voxel core of a voxelization of the shape. We consider a *smooth shape* O as an open set in $\mathbb{R}^3$ that is bounded by a C^2 continuous manifold surface B with a positive *reach* r. The reach [Chazal and Lieutier 2008] is defined as the shortest distance between any point on B to the medial axis of either O or its complement (equivalent to the minimum local feature size [Amenta et al. 2001; Dey and Zhao 2003]). Given a voxel partition of space with voxel size h, we define the voxelization of O as the voxel shape O_h made up all those voxels whose centers lie in O. Such voxelization is also known as the *Gauss digitization* [Lachaud and Thibert 2016]. We denote by B_h, P_h the boundary elements and boundary vertices of O_h. See Figure 5 for an illustration.

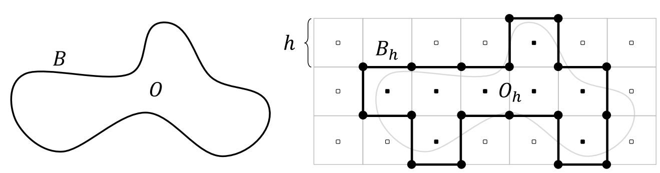

Fig. 5. Notations for voxelization: the smooth shape O with boundary B (left), and voxelization O_h (made up of voxels of size h whose centers are in O) and its boundary set B_h.

3.3.1 Properties of voxelixation. To help establish properties of our approximation, we first present some results that relate the geometry and topology of a voxelization to the smooth shape. These results are variants of, and derived from, existing results in literature [Lachaud and Thibert 2016; Stelldinger et al. 2007].

We first show that the voxelization approximates the smooth shape with bounded Hausdorff distance. Lachaud and Thibert [2016] show that, for voxel sizes smaller than $(2\sqrt{3}/3)r$, the Hausdorff distance between the two boundaries, B_h and B, is bounded by $(\sqrt{3}/2)h$. We build on their result to bound two pairs of geometric structures, which are needed for our analysis of the voxel core: one pair being the boundary vertices P_h of the voxel shape and the smooth surface B, and the other pair being the two shapes O_h and O (see proof in Supplementary Materials):

Theorem 3.9. *For any* $h < \frac{2\sqrt{3}}{3}r$,

(1) $d_H(P_h, B) \leq \frac{\sqrt{2}+\sqrt{3}}{2}h$, *and*

(2) $d_H(O_h, O) \leq \frac{\sqrt{3}}{2}h$.

In addition to being geometrically close to the smooth shape, the voxelization also captures the topology of the shape. Stelldinger et al. [2007] showed that, again for any voxel sizes smaller than $(2\sqrt{3}/3)r$, several variants of the union of voxels (but not the union itself) are all homeomorphic to the original shape O. Building on their result, we show that the voxel shape O_h enjoys a similar property (see proof in Supplementary Materials):

Theorem 3.10. *For any* $h < \frac{2\sqrt{3}}{3}r$, O_h *is homotopy equivalent to* O.

3.3.2 Properties of medial axes approximation. Building on the results above, we can show that the voxel core of a voxelization of a smooth shape is a converging approximation, both topologically and geometrically, of the medial axis of the smooth shape. We denote by C_h the voxel core of the voxelization O_h at voxel size h. Since C_h is homotopy equivalent to O_h (Theorem 3.4), which is in turn homotopy equivalent to O for sufficiently small voxel sizes (Theorem 3.10), it immediately follows that:

Theorem 3.11. *The voxel core* C_h *of the voxelization of a smooth shape* O *with reach* r *is homotopy equivalent to* O *for any* $h < \frac{2\sqrt{3}}{3}r$.

Chazal and Lieutier [2008] have previously considered the general problem of approximating the medial axis of a smooth shape by a subset of the Voronoi diagram of a set of noisy samples. To achieve homotopy equivalence, they require that the Hausdorff distance between the noisy samples and the surface to be less than $r/8$, which yields a much denser sampling than the voxel vertices P_h satisfying $h < (2\sqrt{3}/3)r$. We attribute our generous sampling condition for recovering topology to the regularity of our samples (being voxel vertices).

To bound the distance between the voxel core C_h and the medial axis $\mathcal{M}$, we apply the results by Chazal and Lieutier [2005] on the approximation of the medial axis by the Voronoi diagram of a noisy sample. They define an *ϵ-noisy sample* of a surface B as a finite point set P whose Hausdorff distance with B is less than ϵ. They consider the λ-subset of $VD(P)$, denoted by $VD_\lambda(P)$, whose nearest points in P cannot be fit in a sphere of radius λ. They show that $VD_\lambda(P)$ converges onto the λ-medial axis $\mathcal{M}_\lambda$ as ϵ decreases to zero ([Chazal and Lieutier 2005], Theorem 5). We use this result to show that the λ-subset of the voxel core C_h, denoted by $C_{h,\lambda}$, converges onto the λ-medial axis as the voxel size h decreases to zero. Here, $C_{h,\lambda}$ consists of all points on C_h whose nearest voxel vertices on the boundary cannot fit in a sphere of radius λ.

Theorem 3.12. *For any* $\lambda > 0$ *such that the mapping* $\mathcal{M}(\lambda) = \mathcal{M}_\lambda$ *is continuous at* λ^2, *and any sequence* $\{h_n\}$ *such that* $\lim_{n\to\infty} h_n = 0$,

$$\lim_{n\to\infty} d_H(C_{h_n,\lambda}, \mathcal{M}_\lambda) = 0$$

Proof. By Theorem 3.9 (1), for sufficiently small values of h_n ($< (2\sqrt{3}/3)r$), the sequence P_{h_n} as $n \to \infty$ is a sequence of ϵ-noisy samples of B with decreasing ϵ. To apply the result of Chazal and Lieutier [2005], we need to show that $C_{h_n,\lambda}$ coincides with the λ-subset of the Voronoi diagram of P_{h_n}, denoted by $VD_\lambda(P_{h_n})$, that lies inside the smooth shape O. Note that $C_{h_n,\lambda}$ is the subset of $VD_\lambda(P_{h_n})$ that lies inside the voxelization O_{h_n}. Hence it suffices to show that there is no point $x \in VD_\lambda(P_{h_n})$ that lies either (i) in O but not in O_{h_n}, or (ii) in O_{h_n} but not in O. We will prove this statement by contradiction for any $\lambda > ((\sqrt{2} + 2\sqrt{3})/2)h_n$.

In the case of (i), by Theorem 3.9 (2), there exists a point y on the voxelization boundary B_{h_n} such that $d(x, y) < (\sqrt{3}/2)h_n$. On the other hand, any point on B_{h_n} is no greater than $(\sqrt{2}/2)h_n$ away from a vertex in P_{h_n}. Hence the distance between x and its nearest points in P_{h_n} is at most $(\sqrt{2}/2 + \sqrt{3}/2)h_n < \lambda$, meaning that these nearest points can fit in a sphere (centered at x) of radius less than λ. This contradicts the assumption that x is in the λ-subset $VD_\lambda(P_{h_n})$.

Similarly, in the case of (ii), by Theorem 3.9 (2), there exists a point y on the smooth boundary B such that $d(x, y) < (\sqrt{3}/2)h_n$. On the other hand, by Theorem 3.9 (1), there exists some point P_{h_n} that is less than $((\sqrt{2}+\sqrt{3})/2)h_n$ away from y. Hence the distance between x and its nearest points in P_{h_n} is at most $((\sqrt{2} + 2\sqrt{3})/2)h_n < \lambda$, leading to the same contradiction as above. □

Note that the λ-medial axis $\mathcal{M}_\lambda$ is an increasingly larger subset of $\mathcal{M}$ as λ decreases, and it becomes $\mathcal{M}$ when $\lambda = 0$. Hence, by picking an arbitrarily small λ, Theorem 3.12 ensures that the voxel core converges onto an arbitrarily large subset of the medial axis. In practice, however, we have observed that smaller values of λ lead to slower convergence, as it requires smaller voxel sizes (and hence higher computational cost) to remove noisy components of the voxel core. On the other hand, while larger λ are more effective in removing noise without requiring an excessively high voxel resolution, the resulting approximation may miss important features on the medial axis (e.g., near thin parts of O). Hence the choice of λ controls the trade-off in practice between computational cost and approximation quality. We will demonstrate this trade-off by examples in Section 5.

4 ALGORITHM

The theoretical observations motivate a simple algorithm for approximating the medial axes of both voxel shapes and smooth shapes (see Figure 6):

Step 1: Voxelization If the input is a smooth shape, voxelize the shape at a user-specified voxel size h. By our definition

[2] Chazal and Lieutier [2005] show that this requirement is not overly restrictive: for a smooth shape O, $\mathcal{M}(\lambda)$ is continuous at almost all λ except for a finite number of values.

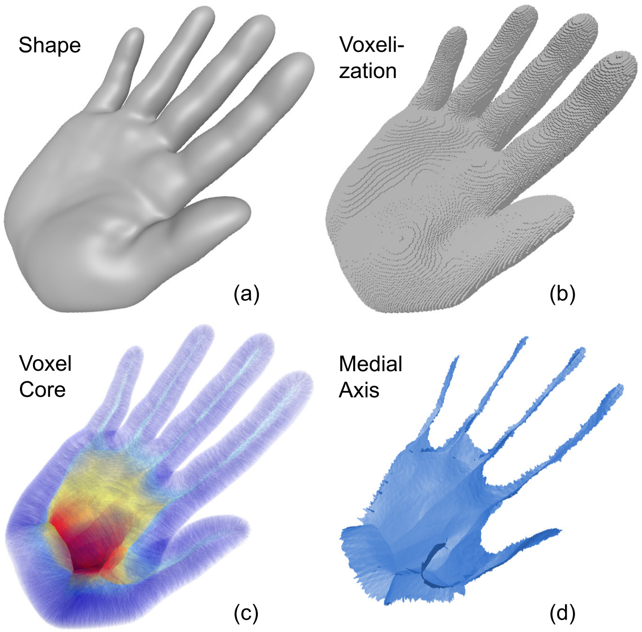

Fig. 6. Algorithm flow: given a non-voxel shape (a), we first voxelize it (b), then extract the voxel core (c, parts with higher radius measure are more opaque and red), and finally prune it to its λ-subset (d).

(Section 3.3), a voxel belongs to the voxelization if its center lies in the input shape.

Step 2: Extracting voxel core Given a voxel shape O, compute the Voronoi diagram of the boundary vertices P, and keep only those Voronoi elements whose vertices lie in O. By Corollary 3.8, these elements make up the voxel core C.

Step 3: λ pruning For each element e in C, compute the radius of the smallest circumscribing sphere of e's nearest points in P. Given a user-specified λ, remove elements in C whose radius value is lower than λ while maintaining the topology of C (see Implementation details below).

If the input is a voxel shape, observations in Section 3.2 ensure that Step 2 computes a thin, enclosed, topologically correct and geometrically close approximation of the medial axis. However, such a medial axis is often highly complex, containing many spurious sheets due to the irregularity on the shape boundary (Figure 6 (c)). Performing Step 3 produces a cleaner subset that are more useful for downstream applications, while the result remains thin, enclosed, and topologically correct.

For smooth input shapes, observations in Section 3.3 guarantee that our algorithm (Steps 1 through 3) produce a medial axis approximation that is thin, homotopy equivalent to the shape (for small enough h), and convergent to the λ-medial axis (as h increases). Compared with existing sampling-based algorithms, our algorithm involves only standard geometric operations, such as voxelization and computing a Voronoi diagram, which can be robustly implemented using off-the-shelf packages (see details below).

Implementation details. For a smooth surface represented as a polyhedral mesh, we perform voxelization using Polymender [Ju 2004]. The tool is very efficient, tolerates mesh defects (e.g., holes and self-intersections), and produces a compact octree representation that can reach high effective voxel resolutions (e.g., 4096^3). In Step 2, we obtain the Voronoi diagram as the dual of the Delaunay triangulation of the boundary vertices P, which we compute by Tetgen [Si 2015]. To maximize robustness, all points of P are given integer coordinates. As there are many instances of 5 or more co-spherical vertices, which result in co-incidental Voronoi vertices, we merge all such vertices in a post-process. In Step 3, we adopt the topology-preserving contraction approach of [Liu et al. 2010], which is designed for any cell complex. We define a *simple pair* as a pair of elements e, f such that e lies on the boundary of f and not on the boundary of any other element. We repeatedly remove a simple pair from the voxel core until no more simple pairs with radius values lower than λ can be found.

Complexity analysis. The complexity of voxelization using Polymender depends on the depth of the octree d, the number of input mesh faces m, and the number of boundary vertices $|P|$ on the output voxel shape. The process takes $O(d(m + |P|))$ time and $O(|P|)$ memory. While the complexity of the Voronoi diagram in 3D can be quadratic in the worst case, it has been shown to be linear for well-distributed points on a surface [Attali and Boissonnat 2004]. In our experiments, we have observed a near-linear complexity for computing the Voronoi diagrams of the voxel boundary points P. As the complexity of the remainder of Steps 2 and 3 is proportional to the size of the Voronoi diagram, these two steps of our algorithm have the complexity of $O(|P|)$.

5 RESULTS

We evaluate our method on different types of inputs, including voxel shapes, smooth shapes, and meshes, and compare with existing medial axis approximation methods. All experiments are conducted on a workstation with 3.47GHz CPU and 24GB memory.

5.1 Voxel shapes

To evaluate the scalability of our algorithm, we first conduct a synthetic experiment that feeds the algorithm with voxelizations of a smooth shape at increasing resolutions (Figure 7). We picked a set of smooth shapes (Ellipsoid, Mug, Elk, Hand, and Fertility) with a diverse range of shape, topology, and space occupancy. Each shape is voxelized at resolutions n^3 where n ranges from 128 to 1280 with an increment of 128. Assuming each shape is scaled to fit in a unit box, we use $\lambda = 0.015$ for Elk (to capture its thin "ear") and $\lambda = 0.025$ for all other shapes.

Observe from the plots that both running time and memory usage of our method scale linearly with the number of boundary vertices $|P|$ (the horizontal axis). Our method can efficiently handle high resolutions, finishing in minutes and using less than 10GB of memory even at the resolution of 1280^3. Note that a significant portion of the running time is spent on computing the Voronoi diagram (using Tetgen).

We compare with two state-of-the-art voxel-based methods, the Hamilton-Jacobi skeleton (HJ) [Siddiqi et al. 2002] and the recent

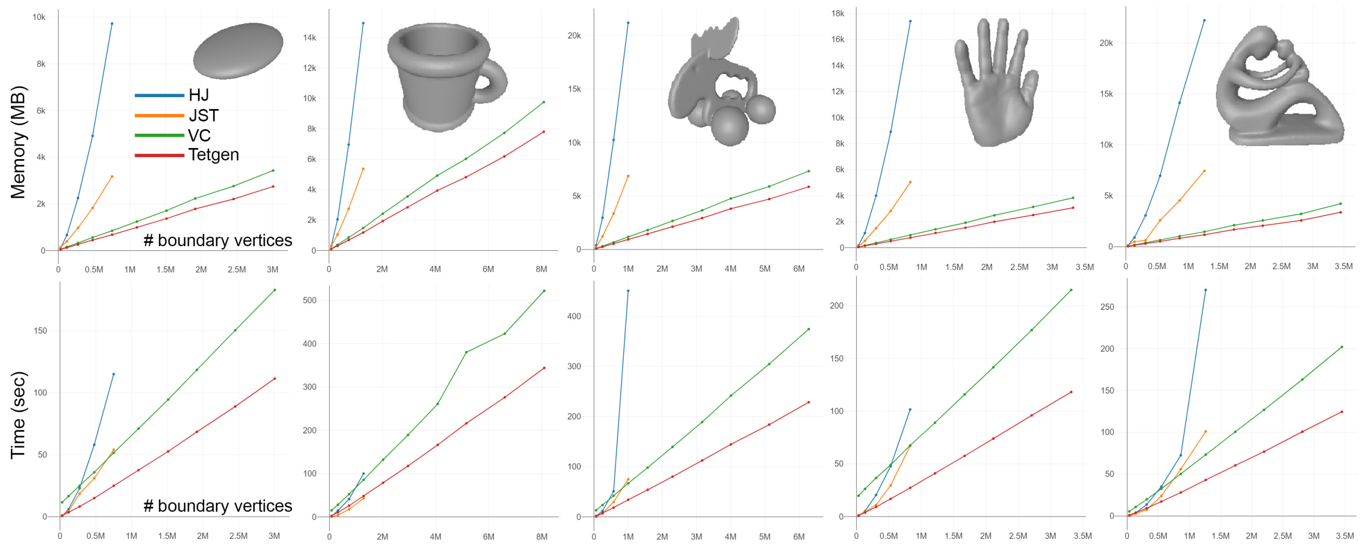

Fig. 7. Performance of our method (VC), the Tetgen component of our method, HJ [Siddiqi et al. 2002] and JST [Jalba et al. 2016] on voxelizations of 5 shapes (shown on top) at increasing voxel resolutions from 128^3 to 1280^3. The horizontal axis is the number of boundary vertices of the voxelization. The plots for HJ and JST end where the implementations ran out of memory or crashed.

work of Jalba et al. (JST) [2016], both of which utilize the Euclidean distance transforms. As seen in the plots in the same figure, both methods exhibit super-linear growth in memory and running time, which significantly limits their capability in handling high resolutions. In particular, HJ quickly exhausts the memory (usually before reaching the resolution of 640^3), while JST crashes at or before reaching 768^3 for every test example.

The scalability of our method makes it suitable for processing biomedical data that often has high resolutions. An example is shown in Figure 8, where the input is a CT scan of a 4-week old corn root at the resolution of $1560 \times 789 \times 1041$. Our method is able to compute the medial axis approximation in less than a minute and using 1.5GB of memory ($\lambda = 0.0025$). As an application, we show the curve skeletons computed from our approximated medial axis using a recent method [Yan et al. 2016] (Figure 8 bottom). This method takes in an initial medial axis and extracts a curve subset guided by a measure computed on the medial axis. Observe that the curve skeleton reveals the branching structure of the root, which is particularly useful for plant biologists to understand the root system architecture.

5.2 Smooth shapes

We first evaluate the effect of voxel resolution and parameter λ on the approximation result (Figure 9). We use an Ellipsoid shape (Figure 7 top-left) for which the ground truth medial axis can be computed for comparison (its boundary is indicated by a red outline). As promised by our analysis (Section 3.4), for any value of λ, our approximation converges to a subset of the medial axis as the voxel resolution increases. Larger values of λ allow faster convergence, resulting in cleaner approximations even at low voxel resolutions, but the converged results cover smaller portions of the medial axis (see the gap between the outline of the medial axis and our approximation at $\lambda = 0.085$). As a result, the choice of voxel resolution (or voxel size h) and λ controls the trade-off between computational efficiency and approximation quality. In particular, a large λ coupled with a low resolution allows fast computation but may miss portions of the medial axis where the radius measure is low. On the other hand, a small λ coupled with a high resolution gives accurate approximation of the medial axis but at a higher computational cost.

Next we compare our method with three state-of-the-art sampling-based methods whose implementations are available: the Voronoi pruning method of Dey and Zhao (DZ) [2003], the power crust (PC) [Amenta et al. 2001], and the union-of-ball method [Amenta and Kolluri 2001] (we use the implementation in the Scale Axis Transform (SAT) [Miklos et al. 2010] by setting the scale parameter to $s = 1.0$). We use the default sampling distance in SAT, which is 0.01, and feed the same set of samples to all three sampling-based methods. The results are shown in Figure 10, together with performance statistics and topological numbers of the results (e.g., Euler characteristics and number of connected components).

Observe that our method can produce approximations that are visually similar to these sampling-based methods, but often at the cost of more time and memory. Although both our method and sampling-based methods rely on Voronoi diagrams, the former uses samples (voxel vertices) that are generally off the surface while the latter sample directly on the surface. Therefore, to achieve similar proximity to the medial axis, our method generally requires more samples, which leads to higher computational cost.

The key advantage of our method is its robustness in capturing the topology. Observe from Figure 10 that the Voronoi pruning method (DZ) generates numerous isolated components. The power crust (PC) produces a large number of duplicated triangles as well

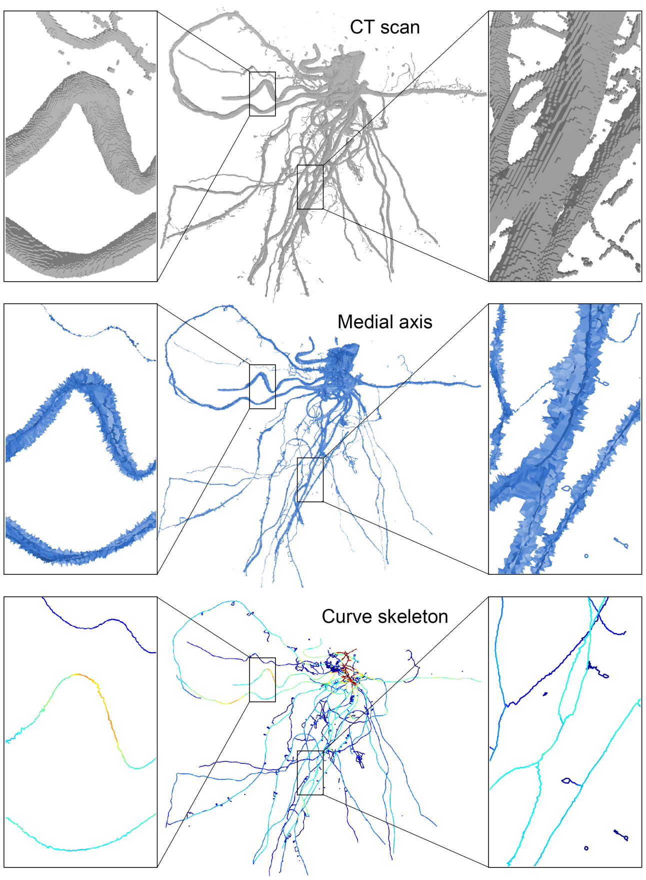

Fig. 8. A high-resolution CT scan of a corn root (top), medial axis computed by our method (middle), and a curve skeleton produced by [Yan et al. 2016] from our medial axis (bottom, color indicates thickness of shape around each curve skeleton point).

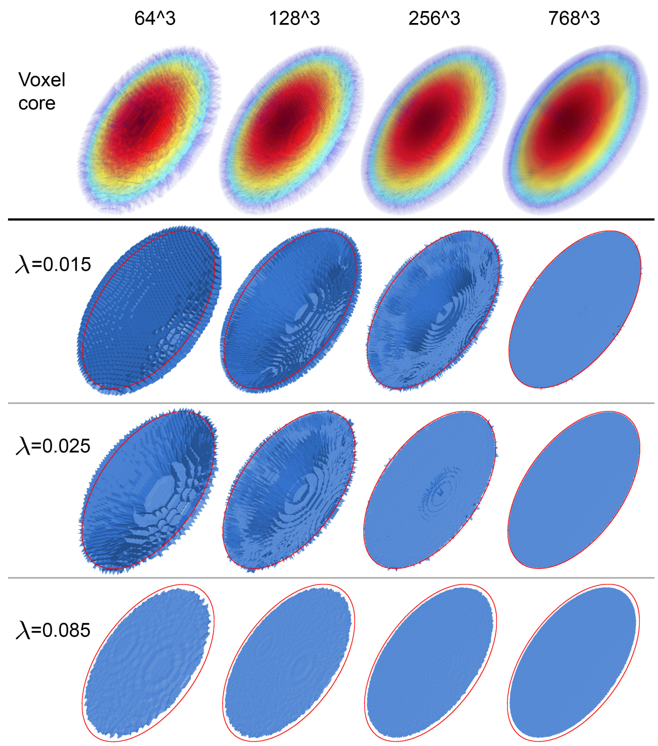

Fig. 9. Approximating the medial axis of an Ellipsoid at increasing voxelization resolution (left ro right) and λ (top to bottom). The first row shows the un-pruned voxel core colored by radius measure (higher radii are more red and opaque). Red outlines mark the boundary of the true medial axis.

as closed "pockets" (triangles forming closed cavities), resulting in extremely high Euler characteristics. While the union-of-ball method is theoretically guaranteed to be topologically correct, the implementation (SAT) produces many closed pockets as well, as evident in the incorrect Euler characteristics. We have found that these topological errors do not go away as the sampling rate increases. In contrast, our method captures the correct topology of these shapes for any voxel resolution at or beyond 256^3.

Although the topological artifacts produced by sampling-based methods are often tiny and hard to see, they can be detrimental for downstream operations on the medial axis. One of such operations is computing simplified skeletal descriptors, such as a curve skeleton or a surface skeleton [Tagliasacchi et al. 2016]. Algorithms for computing skeletons often work by pruning a given medial axis while preserving its topology. Topological errors on the medial axis, no matter how small, can prevent these algorithms from being able to fully simplify the medial axis. We compare in Figure 11 the skeletons computed by two recent skeletonization algorithms [Li et al. 2015; Yan et al. 2016] on two sets of medial axes, ones produced by SAT and containing topological errors, and ones produced by our method with the correct topology. Observe that the skeletons computed from the SAT medial axes contain many noisy branches. At the end of each such branch lies a "pocket" in the input medial axis, which cannot be removed without causing a topological change.

Besides producing topological artifacts, another drawback of existing implementations of sampling-based methods is that they often need an excessive number of samples to capture thin features on the shape. For example, to reproduce the thin connections on the "tanglecube" shape in Figure 12 (a), SAT needs nearly half a million sample points, and the computation takes more than ten minutes (Figure 12 (b,c)). In contrast, our method preserves these connections at voxel resolutions as low as 256^3 ($\lambda = 0.03$) (Figure 12 (d)). Increasing the resolution to 512^3 produces a much better geometric approximation to the medial axis that is comparable with SAT, but with the correct topology and a shorter computing time (just over a minute). Our advantage in efficiency in this example owes to the generous sampling condition for achieving topology preservation (Theorem 3.11).

5.3 Meshes

Even though theoretical guarantees are given only for voxel and smooth shapes, our method can process any boundary representations (e.g., meshes). We show several examples in Figure 13 computed at voxel resolution 1024^3 ($\lambda = 0.025$ for all these examples).

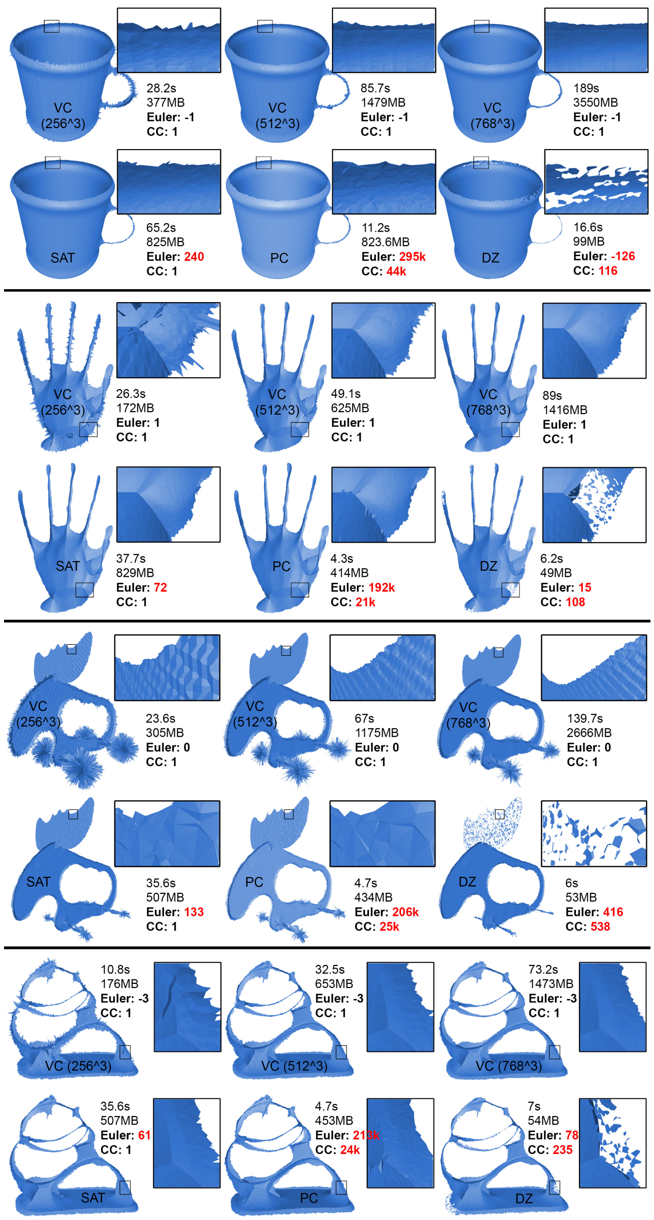

Fig. 10. Comparing our method (VC) at resolutions 256^3, 512^3, 768^3 and three sampling-based methods, SAT [Amenta and Kolluri 2001; Miklos et al. 2010], PC [Amenta et al. 2001], and DZ [Dey and Zhao 2003] on several smooth shapes. Running time (in seconds) and memory usage (in MB) are reported for each method, as well as the Euler characteristic and number of connected components (incorrect numbers are marked red).

Even at this high resolution (which exceeds the capability of voxel-based methods such as HJ and JST), our program finishes in under 3 minutes and uses less than 5GB memory for each shape. In all these examples, we found that the results faithfully capture the topology of these shapes.

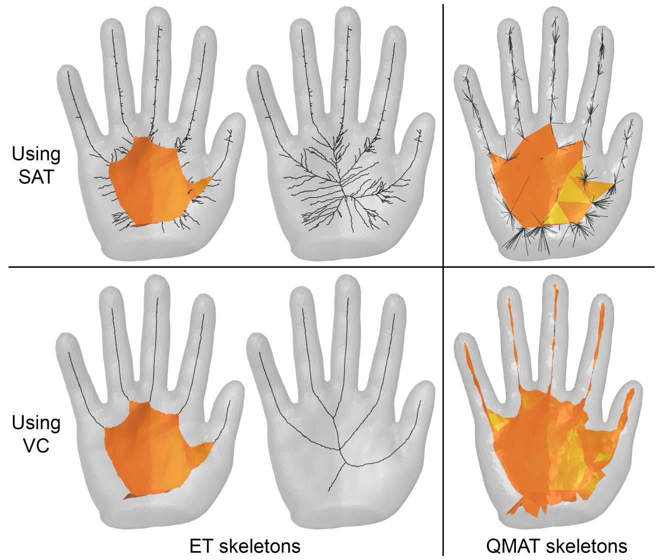

Fig. 11. Comparing skeletons computed by ET [Yan et al. 2016] (two skeletons are shown with different parameter settings) and QMAT [Li et al. 2015] using input medial axes given by SAT [Miklos et al. 2010] and our method (VC). The noisy branches in the skeletons computed from the SAT medial axes are due to the presence of tiny pockets in the medial axes.

The scalability of our method allows it to run at very high voxel resolutions. Coupled with a smaller value λ, we can afford to compute accurate approximations of the medial axis even for complex shapes. As shown in Figure 14, running our method at the resolution of 2048^3 creates more detailed and smoother medial axis for the Neptune model.

6 CONCLUSION AND DISCUSSION

In this paper, we present a novel algorithm for computing the medial axes of 3D shapes that is simple, scalable, numerically robust, and provably correct (for voxel and smooth shapes). The algorithm is based on the observations that the medial axis of a voxel can be well approximated by the interior Voronoi diagram of the boundary vertices (the voxel core), and that the voxel cores converge to the medial axis of any smooth shape under increasing resolutions of voxelization. We present experimental evidence that our method is more scalable than existing voxel-based methods while being a more robust alternative to existing sampling-based methods. The code and data are available online at https://yajieyan.github.io/project/voxelcore/.

Limitation and future work. There are a number of limitations of our work and avenues for future research. First, although our method is more robust than sampling-based methods in terms of topology, achieving a comparable geometric accuracy as sampling-based methods requires our method to work with fine voxel resolutions and hence incurring higher computational cost. It would be interesting to explore means to improve the geometry of our approximation without increasing voxel resolution, for example by a geometric deformation towards the medial axis. Second, while our method can handle much larger voxel volumes than existing

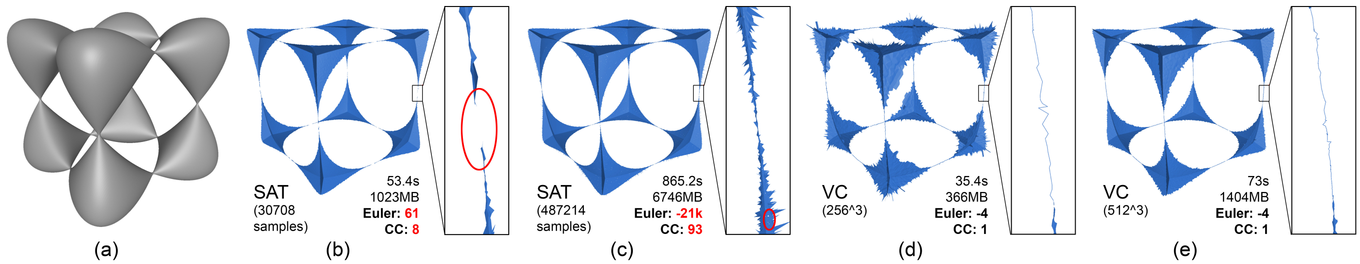

Fig. 12. Comparing SAT [Miklos et al. 2010] and our method (VC) on a shape with thin connections (the shape is *not* aligned with the coordinate axes) (a). At a typical sampling rate (b), SAT misses the thin connections (highlighted). To capture the connections, SAT requires a high sampling rate and computational cost (c), but at the same time produces topological artifacts such as holes (highlighted). Our method captures the correct topology of the input shape using voxel resolutions as low as 256^3 (d,e), using much less memory and time than SAT.

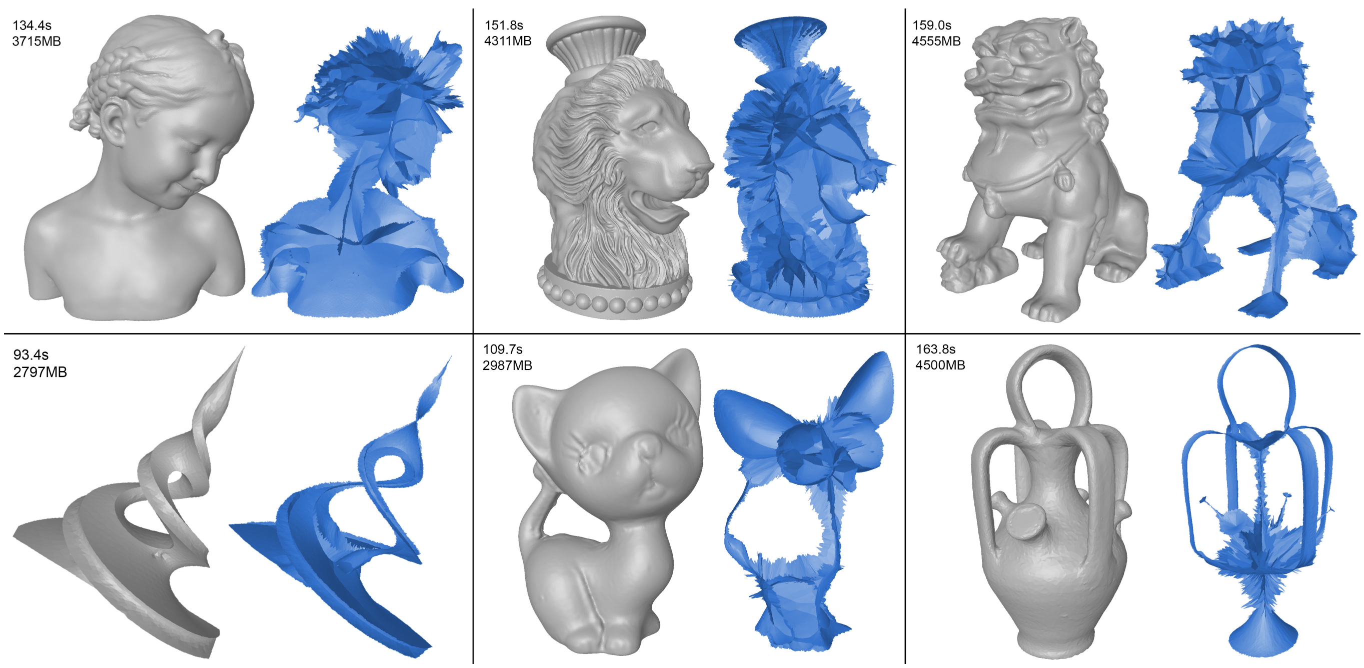

Fig. 13. Approximating the medial axes of meshes (at voxel resolution 1024^3).

voxel-based methods, its linear growth of computational cost makes it challenging to handle even larger volumes. Such data could come from high-resolution biomedical imaging or voxelizing shapes that contain extremely thin features (e.g., wires and sheets). To come up with a truly scalable method, a promising idea is to replace uniform-sized voxels on a regular grid with non-uniform voxels on an adaptive octree grid, so that the size of the voxels adapts to the scale of local features. Extending this work to the non-uniform setting opens up many interesting questions, both in theory and algorithms. Lastly, we are interested in investigating extension of our theoretical results to higher dimensions.

ACKNOWLEDGMENTS

This work is supported by the National Science Foundation, under grants IIS-1302200, DBI-1356388, RI-1618685. The authors would like to thank Aim@Shape Project for providing the 3D mesh models and Christopher Topp for providing the root CT scan. The authors also want to thank the anonymous reviewers for their helpful suggestions.

REFERENCES

Nina Amenta, Sunghee Choi, and Ravi Krishna Kolluri. 2001. The power crust, unions of balls, and the medial axis transform. *Computational Geometry* 19, 2-3 (2001), 127–153.

Nina Amenta and Ravi Krishna Kolluri. 2001. The medial axis of a union of balls. *Comput. Geom.* 20, 1-2 (2001), 25–37.

Carlo Arcelli and Gabriella Sanniti di Baja. 1993. Euclidean skeleton via centre-of-maximal-disc extraction. *Image and Vision Computing* 11, 3 (1993), 163–173.

Carlo Arcelli, Gabriella Sanniti di Baja, and Luca Serino. 2011. Distance-driven skeletonization in voxel images. *IEEE Transactions on Pattern Analysis and Machine Intelligence* 33, 4 (2011), 709–720.

Dominique Attali and Jean-Daniel Boissonnat. 2004. A linear bound on the complexity of the Delaunay triangulation of points on polyhedral surfaces. *Discrete &*

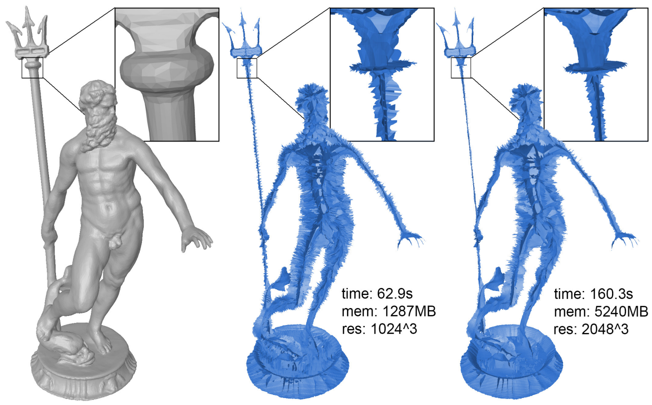

Fig. 14. Medial axes of Neptune computed at high voxel resolutions.

Computational Geometry 31, 3 (2004), 369–384.

Dominique Attali and Annick Montanvert. 1996. Modeling noise for a better simplification of skeletons. In *Proceedings 1996 International Conference on Image Processing, Lausanne, Switzerland, September 16-19, 1996.* 13–16.

Gilles Bertrand and Grégoire Malandain. 1994. A new characterization of three-dimensional simple points. *Pattern Recognition Letters* 15, 2 (1994), 169–175.

Anders Björner, Bernhard Korte, and László Lovász. 1985. Homotopy properties of greedoids. *Advances in Applied Mathematics* 6, 4 (1985), 447–494.

H. Blum. 1967. A transformation for extracting new descriptors of form. *Models for the Perception of Speech and Visual Form* (1967), 362–80.

J. Brandt and V. Algazi. 1992. Continuous skeleton computation by Voronoi diagram. *CVGIP: Image Understanding* 55, 3 (1992), 329 – 338.

Frederic Cazals, Aditya Parameswaran, and Sylvain Pion. 2008. Robust construction of the three-dimensional flow complex. In *Proceedings of the twenty-fourth annual symposium on Computational geometry.* ACM, 182–191.

Frédéric Chazal and André Lieutier. 2005. The "λ-medial axis". *Graphical Models* 67, 4 (2005), 304–331.

Frédéric Chazal and André Lieutier. 2008. Smooth manifold reconstruction from noisy and non-uniform approximation with guarantees. *Computational Geometry* 40, 2 (2008), 156–170.

Tim Culver, John Keyser, and Dinesh Manocha. 2004. Exact computation of the medial axis of a polyhedron. *Computer Aided Geometric Design* 21, 1 (2004), 65–98.

Tamal K. Dey and Wulue Zhao. 2003. Approximating the Medial Axis from the Voronoi Diagram with a Convergence Guarantee. *Algorithmica* 38, 1 (2003), 179–200.

Michal Etzion and Ari Rappoport. 2002. Computing Voronoi skeletons of a 3-D polyhedron by space subdivision. *Computational Geometry* 21, 3 (2002), 87–120.

Mark Foskey, Ming C Lin, and Dinesh Manocha. 2003. Efficient computation of a simplified medial axis. In *Proceedings of the eighth ACM symposium on Solid modeling and applications.* ACM, 96–107.

Yaorong Ge and J Michael Fitzpatrick. 1996. On the generation of skeletons from discrete Euclidean distance maps. *IEEE Transactions on Pattern Analysis and Machine Intelligence* 18, 11 (1996), 1055–1066.

Joachim Giesen, Edgar A Ramos, and Bardia Sadri. 2006. Medial axis approximation and unstable flow complex. In *Proceedings of the twenty-second annual symposium on Computational geometry.* ACM, 327–336.

Wim H Hesselink and Jos BTM Roerdink. 2008. Euclidean skeletons of digital image and volume data in linear time by the integer medial axis transform. *IEEE Transactions on Pattern Analysis and Machine Intelligence* 30, 12 (2008), 2204–2217.

Christoph M Hoffmann. 1990. How to construct the skeleton of CSG objects. (1990).

Andrei C Jalba, Jacek Kustra, and Alexandru C Telea. 2013. Surface and curve skeletonization of large 3D models on the GPU. *IEEE transactions on pattern analysis and machine intelligence* 35, 6 (2013), 1495–1508.

Andrei C Jalba, Andre Sobiecki, and Alexandru C Telea. 2016. An unified multiscale framework for planar, surface, and curve skeletonization. *IEEE transactions on pattern analysis and machine intelligence* 38, 1 (2016), 30–45.

Tao Ju. 2004. Robust repair of polygonal models. *ACM Transactions on Graphics (TOG)* 23, 3 (2004), 888–895.

Reinhard Klette and Azriel Rosenfeld. 2004. *Digital geometry: Geometric methods for digital picture analysis.* Elsevier.

Jacques-Olivier Lachaud and Boris Thibert. 2016. Properties of gauss digitized shapes and digital surface integration. *Journal of Mathematical Imaging and Vision* 54, 2 (2016), 162–180.

Yong-Gu Lee and Kunwoo Lee. 1997. Computing the medial surface of a 3-D boundary representation model. *Advances in Engineering Software* 28, 9 (1997), 593–605.

Pan Li, Bin Wang, Feng Sun, Xiaohu Guo, Caiming Zhang, and Wenping Wang. 2015. Q-MAT: Computing Medial Axis Transform By Quadratic Error Minimization. *ACM Trans. Graph.* 35, 1 (Dec. 2015), 8:1–8:16.

André Lieutier. 2003. Any Open Bounded Subset of Rn Has the Same Homotopy Type Than Its Medial Axis. In *Proceedings of the Eighth ACM Symposium on Solid Modeling and Applications (SM '03).* 65–75.

L. Liu, Erin W. Chambers, David Letscher, and T. Ju. 2010. A simple and robust thinning algorithm on cell complexes. *Comput. Graph. Forum* 29, 7 (2010), 2253–2260.

Jaehwan Ma, Sang Won Bae, and Sunghee Choi. 2012. 3D medial axis point approximation using nearest neighbors and the normal field. *The Visual Computer* 28, 1 (2012), 7–19.

Balint Miklos, Joachim Giesen, and Mark Pauly. 2010. Discrete Scale Axis Representations for 3D Geometry. *ACM Trans. Graph.* 29, 4 (July 2010), 101:1–101:10.

Victor Milenkovic. 1993. Robust Construction of the Voronoi Diagram of a Polyhedron.. In *CCCG*, Vol. 93. 473–478.

Suraj Musuvathy, Elaine Cohen, and James Damon. 2011. Computing medial axes of generic 3D regions bounded by B-spline surfaces. *Computer-Aided Design* 43, 11 (2011), 1485–1495.

Kálmán Palágyi and Attila Kuba. 1999. A parallel 3D 12-subiteration thinning algorithm. *Graphical Models and Image Processing* 61, 4 (1999), 199–221.

Chris Pudney. 1998. Distance-ordered homotopic thinning: a skeletonization algorithm for 3D digital images. *Computer Vision and Image Understanding* 72, 3 (1998), 404–413.

M Ramanathan and B Gurumoorthy. 2010. Interior Medial Axis Transform computation of 3D objects bound by free-form surfaces. *Computer-Aided Design* 42, 12 (2010), 1217–1231.

Dennie Reniers, Jarke van Wijk, and Alexandru Telea. 2008. Computing Multiscale Curve and Surface Skeletons of Genus 0 Shapes Using a Global Importance Measure. *IEEE Transactions on Visualization and Computer Graphics* 14, 2 (2008), 355–368.

Martin Rumpf and Alexandru Telea. 2002. A continuous skeletonization method based on level sets. In *Proceedings of the symposium on Data Visualisation 2002.* Eurographics Association, 151–ff.

Punam K Saha, Gunilla Borgefors, and Gabriella Sanniti di Baja. 2016. A survey on skeletonization algorithms and their applications. *Pattern Recognition Letters* 76 (2016), 3–12.

Punam K. Saha and Bidyut Baran Chaudhuri. 1994. Detection of 3-D simple points for topology preserving transformations with application to thinning. *IEEE transactions on pattern analysis and machine intelligence* 16, 10 (1994), 1028–1032.

Evan C. Sherbrooke, Nicholas M. Patrikalakis, and Erik Brisson. 1996. An Algorithm for the Medial Axis Transform of 3D Polyhedral Solids. *IEEE Transactions on Visualization and Computer Graphics* 2, 1 (1996), 44–61.

Hang Si. 2015. TetGen, a Delaunay-based quality tetrahedral mesh generator. *ACM Transactions on Mathematical Software (TOMS)* 41, 2 (2015), 11.

Kaleem Siddiqi, Sylvain Bouix, Allen Tannenbaum, and Steven W. Zucker. 2002. Hamilton-Jacobi Skeletons. *International Journal of Computer Vision* 48, 3 (July 2002), 215–231.

Kaleem Siddiqi and Stephen M. Pizer. 2008. *Medial Representations.* Springer.

André Sobiecki, Andrei Jalba, and Alexandru Telea. 2014. Comparison of curve and surface skeletonization methods for voxel shapes. *Pattern Recognition Letters* 47 (2014), 147–156.

Peer Stelldinger, Longin Jan Latecki, and Marcelo Siqueira. 2007. Topological equivalence between a 3D object and the reconstruction of its digital image. *IEEE transactions on pattern analysis and machine intelligence* 29, 1 (2007).

Svetlana Stolpner and Kaleem Siddiqi. 2006. Revealing significant medial structure in polyhedral meshes. In *3D Data Processing, Visualization, and Transmission, Third International Symposium on.* IEEE, 365–372.

Avneesh Sud, Liangjun Zhang, and Dinesh Manocha. 2006. *Homotopy Preserving Approximate Voronoi Diagram of 3D Polyhedron.* Technical Report. Technical report.

Andrea Tagliasacchi, T. Delame, M. Spagnuolo, N. Amenta, and A. Telea. 2016. 3D Skeletons: A State-of-the-Art Report. In *Eurographics.*

Roger C. Tam and Wolfgang Heidrich. 2003. Shape Simplification Based on the Medial Axis Transform. In *14th IEEE Visualization 2003 Conference (VIS 2003), 19-24 October 2003, Seattle, WA, USA.* 481–488.

YF Tsao and King Sun Fu. 1981. A parallel thinning algorithm for 3-D pictures. *Computer graphics and image processing* 17, 4 (1981), 315–331.

Yajie Yan, Kyle Sykes, Erin Chambers, David Letscher, and Tao Ju. 2016. Erosion thickness on medial axes of 3D shapes. *ACM Transactions on Graphics (TOG)* 35, 4 (2016), 38.